<u>Supporting Information</u>

Amazingly enhancement of OER performances: Creating a well-designed functional Ni and N-doped carbon layer as support material for fabricating a NiFe-LDH electrocatalyst

Yu Wei,[a] Zhenze Han,[a] Taolue Liu,[a] Xin Ding,[*b] and Yan Gao[*a]

[a.]State Key Laboratory of Fine Chemicals, Frontier Science Center for Smart Materials, School of Chemical Engineering, Dalian University of Technology, Dalian 116024, China. E-mail: dr.gaoyan@dlut.edu.cn

[b.]College of Chemistry and Chemical Engineering, Qingdao University, Qingdao, 266071, Shandong, China. E-mail: dingxin@qdu.edu.cn

Experimental

1. General materials

p-nitrobenzaldehyde (98%), lactic acid (99%), pyrrole (99%), $SnCl_2 \cdot 2H_2O$ (99%), pyridine (99.5%), $TBA(PF_6)$ (99%), acetonitrile (ACN, 99.9%), $Ni(NO_3)_2 \cdot 6H_2O$ (98%) and $FeSO_4 \cdot 7H_2O$ (99%) were purchased from Innochem chemical company; Nitrobenzene (99%) and KOH (95%) were purchased from Aladdin chemical company; Toray carbon papers (CP, TGP-H-060) were purchased from Alfa Aesar; Deionized water (18 MΩ·cm resistivity) was used for preparing all aqueous solutions; The other materials come from industrial-grade products.

2. Synthetic methods and fabrication of the electrodes

2.1. Synthesis of tetrakis(4-aminophenyl)porphyrin (TAPP): The synthesis of TAPP was referred to reference,[1] and produced a dark purple powder (13.6% yield in two steps). ^{1}H NMR (500 MHz, d-DMSO): δ 8.89 (s, 8H, pyrrolering), 7.86 (d, 8H, ArH), 7.01 (d, 8H, ArH), 5.57 (s, 8H, NH2), -2.73 (s, 2H, pyrrole NH). ^{13}C NMR (126 MHz, d-DMSO): δ 148.45, 135.39, 130.89, 128.75, 120.52, 112.50. ESI-MS: calcd. for $C_{44}H_{34}N_8$ $[M + H]^+$ 675.3, found 675.3.

2.2. Synthesis of [tetra(4-aminophenyl)porphyrin] nickel (NiTAPP): To a stirring solution of TAPP (135 mg, 0.2 mmol) in DMF (30 mL) was added Nickel acetate tetrahydrate (55 mg, 0.22 mmol). The reaction mixture was heated up to reflux temperature for 6 hours under Ar atmosphere. After cooling to room temperature, 30 mL of distilled water was added, and continue to stir for 1 hour. Yield 90.5%. ^{1}H NMR (500 MHz, d-DMSO): δ 8.79 (s, 8H, pyrrolering), 7.64 (d, 8H, ArH), 6.93 (d, 8H, ArH), 5.50 (s, 8H, NH2). ^{13}C NMR (126 MHz, d-DMSO): δ 148.47, 142.40, 134.39, 131.76, 127.33, 119.47, 112.60. ESI-MS: calcd. for $C_{44}H_{32}N_8Ni$ 730.2, found 730.3.
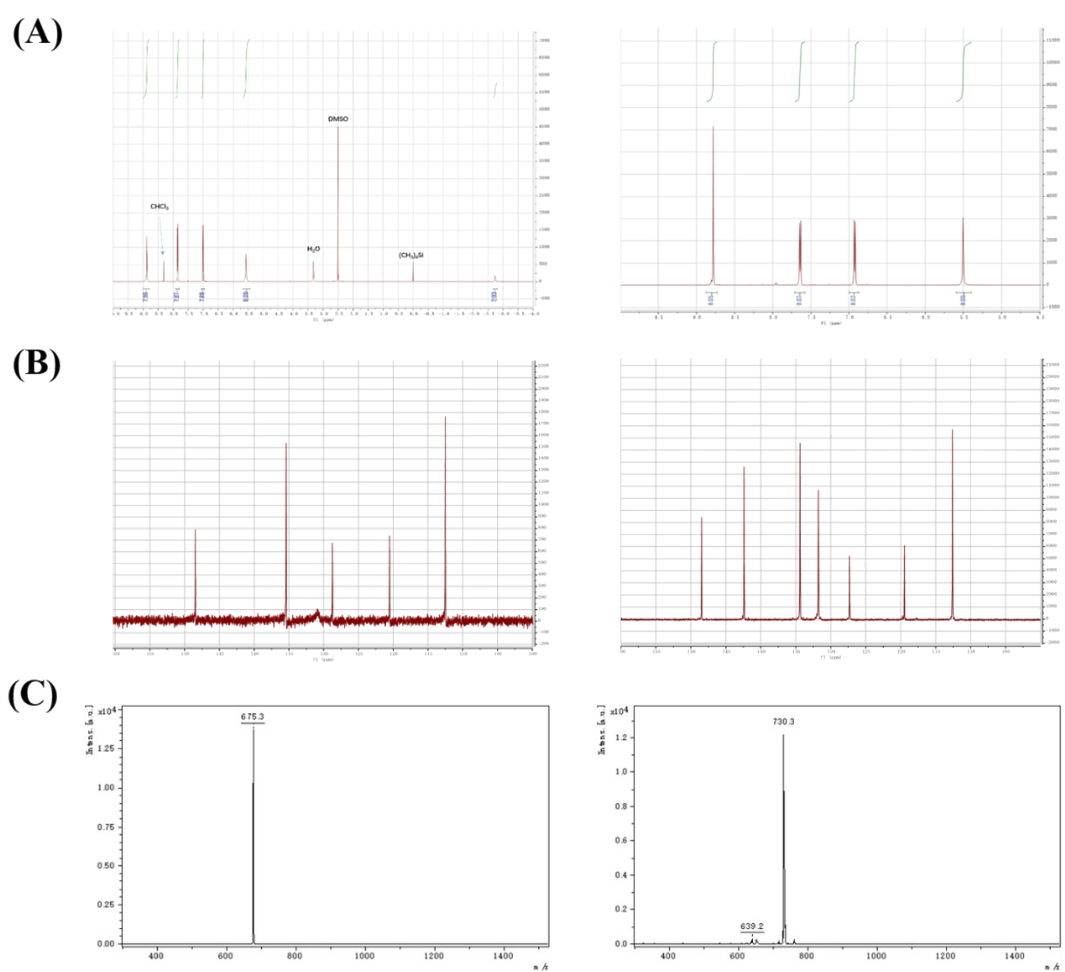
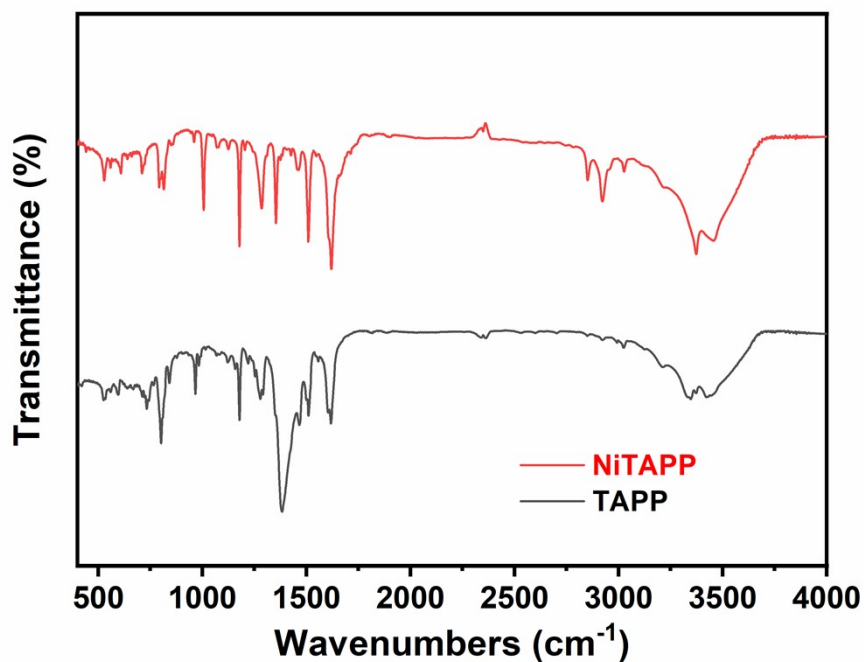**Figure S1.** (A) ^{1}H NMR, (B) ^{13}C NMR, (C) Mass spectra of TAPP and NiTAPP

**Figure S2.** IR spectra of TAPP and NiTAPP

Table S1. IR peak coordinates of TAPP and NiTAPP

Vibration modes	TAPP (cm^{-1})	NiTAPP (cm^{-1})
Disubstituted phenyl-out of plane	731	715
Disubstituted phenyl-out of plane	799	803
Pyrrolic ring deformation and breathing	963	958
Phenyl ring deformation	983	1005
-C-H deformation phenyl ring	1178	1178
Stretching -C-NH$_2$ aromatic amine	1283	1285
Stretching -C-N aromatic amine	1381	1354
Tetrapyrrole C-C-N-C	1467	1460
Tetrapyrrole C-C-N-C	1511	1509
Amino N-H deformation	1605	1606
NH$_2$ scissoring	1618	1620

2.3. Electropolymerization of NiTAPP: P-NiTAPP was electropolymerized as detailed below: A solution of 0.25 mM NiTAPP in ACN was prepared, containing 5% v/v pyridine as a neutralizing agent, and 0.05 M tetrabutylammonium hexafluorophosphate TBA(PF$_6$) as the supporting electrolyte. The electropolymerization was performed in a three-electrode electrochemical cell and CP as working electrodes (1 cm×1 cm). Pt mesh was used as the counter electrode. Ag/AgNO$_3$ reference electrodes were prepared in the laboratory. The potential was swept from -0.1 V to 0.3 V vs. Ag/AgNO$_3$ at scan rates of 2 mV/s for 8 cycles, as shown in Figure S2. Then the finished P-NiTAPP/CP was washed with acetonitrile and dried naturally.
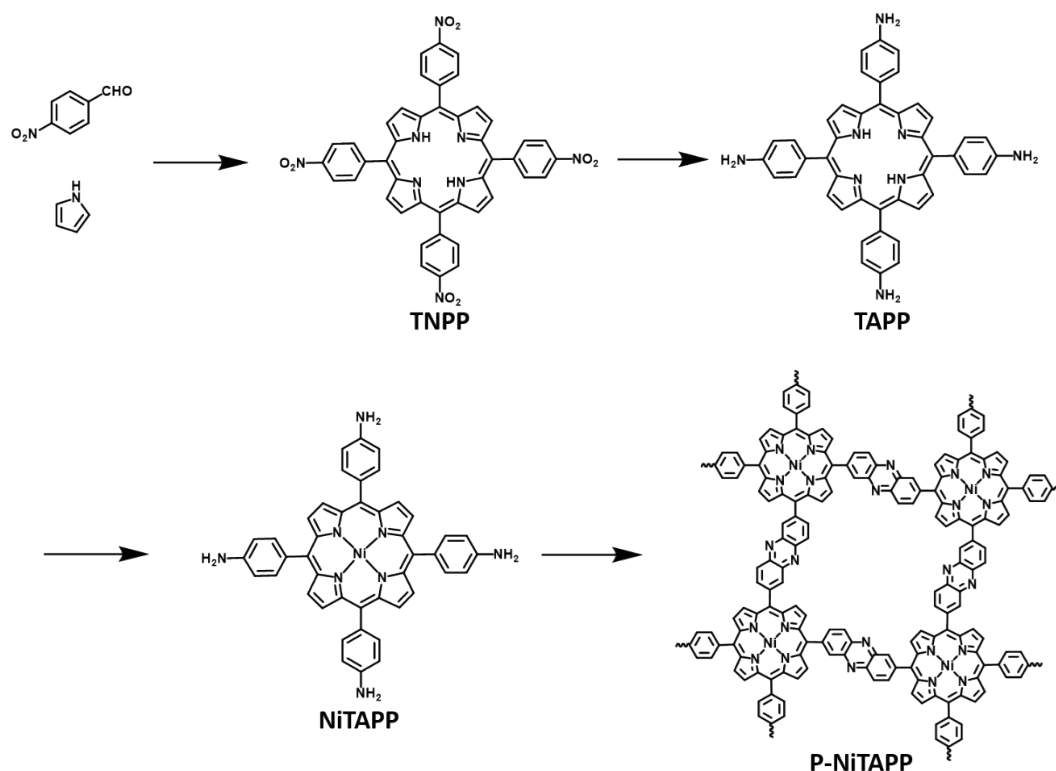
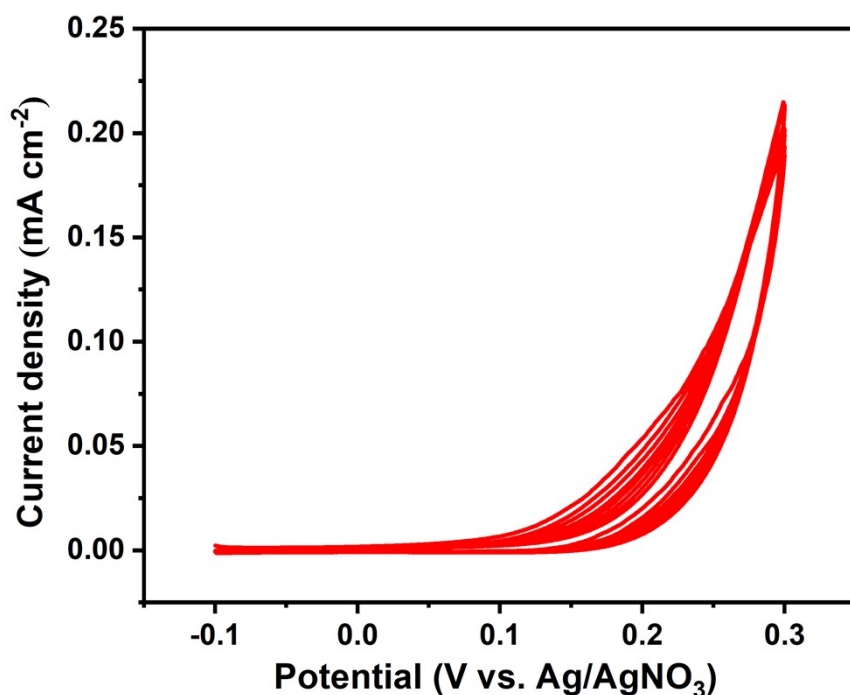**Scheme S1.** The reaction scheme of P-NiTAPP synthesis.

Figure S3. Cyclic voltammogram traces of NiTAPP electropolymerization on CP.

2.4. Fabrication of NiFe-LDH/NNC/CP electrode

The NNC/CP (Ni and N-doped dense carbon layer) electrode was prepared by carbonization of P-NiTAPP coated on CP. Specific conditions are as follows: the P-NiTAPP/CP was then calcinated at 500 °C for 1.5 h at a heating rate of 5 °C /min under Ar atmosphere. The electrodeposition of NiFe-LDH was carried out in a three-electrode configuration, by using as-prepared NNC/CP, Pt net, and silver chloride electrode (Ag/AgCl) as the working, counter, and reference electrode, respectively. The fresh electrolyte was obtained by dissolving $Ni(NO_3)_2 \cdot 6H_2O$ (0.15 M) and $FeSO_4 \cdot 7H_2O$ (0.15 M) in 20 mL water. The applied potential was -0.76 V vs. NHE, with different electrodeposition time of 50, 100 and 150 s to control the amount of the NiFe-LDH. The samples were then washed with deionized water and dried in the air[2].

2.5. Fabrication of NiFe-LDH/NC/CP and NiFe-LDH/ CP

For comparison, NiFe-LDH was synthesized on NC/CP (N-doped dense carbon layer) and CP by the same method as fabrication of NiFe-LDH/NNC/CP. The fabrication condition of NC is exactly the same as those of NNC, except that NiTAPP was especially replaced by TAPP.

3. Material characterization

The morphology and dimension of as-prepared materials were characterized by Nova NanoSEM

450 equipment. The microstructures of the samples were characterized by TEM (FEI TF30). X-ray diffraction (XRD) pattern was collected by a D/max-2400 diffractometer (Japan Rigaku Rotaflex) using Cu Kα radiation (λ = 154.1 nm). X-ray photoelectron spectroscopy (XPS) measurement was performed on a Thermo ESCALAB XI+ instrument. The binding energy (BE) was calibrated with respect to the C 1s level (284.8 eV) of adventitious carbon. Video optical contact Angle measuring instrument (dataphysics/OCA50, DATAPHYSICS) was used to measure the surface wettability of the electrodes.

4. Electrochemical measurements

All the electrochemical measurements were performed by CHI 660E Electrochemical Analyzer (Shanghai Chenhua Instrument Co., Ltd) with a three-electrode system in 1M KOH solution (pH = 13.6) at room temperature. A 1cm^2 of CP decorated with catalyst was used as working electrode, Pt mesh and HgO/Hg electrode were used as counter and reference electrodes, respectively. All the potentials were converted to reversible hydrogen electrode (RHE) scale, $E_{RHE} = E_{HgO/Hg} + 0.059pH + 0.098$ V.

Before measurements, the working electrode was activated at constant current densities of 20 mA cm^{-2} for 10 min. Linear sweep voltammetry (LSV) curves corrected with iR-compensation were tested at a scan rate of 5 mV/s. The chronopotentiometry curve was achieved for current densities of 50 mA cm^{-2} without iR-compensation. Tafel slopes were calculated by plotting overpotential against log (current density) with iR compensation. The electrochemical impedance spectroscopy (EIS) was recorded at the overpotential of 230 mV at the amplitude of the sinusoidal voltage of 5 mV over a frequency range from 0.01 Hz to 100 Hz. Cyclic voltammetry (CV) curves were collected at different scan rates in a non-Faradic region to evaluate the double-layer capacitance values (C_{dl}).

$$Cdl = ic/v \qquad \text{Equation S1}$$

$$ECSA = Cdl/Cs \qquad \text{Equation S2}$$

Where ic represents the charging current, v is the scan rate, Cs is the specific capacitance (0.040 mF/cm2), S is the geometric area of the electrode (1 cm^2).
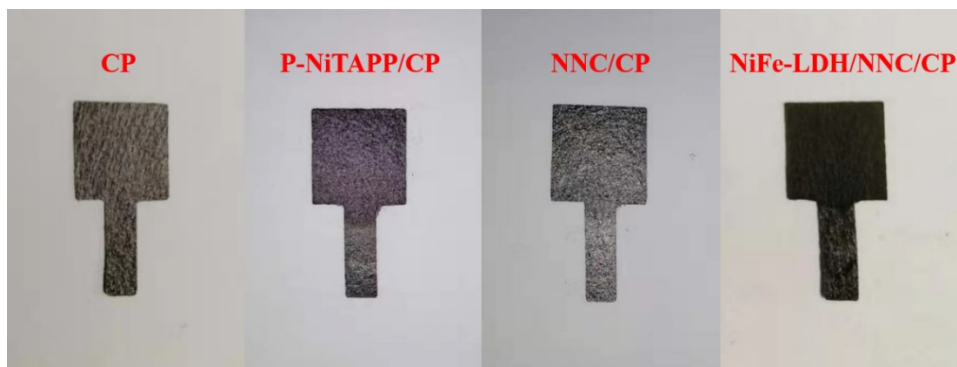
5. Supplementary Figures

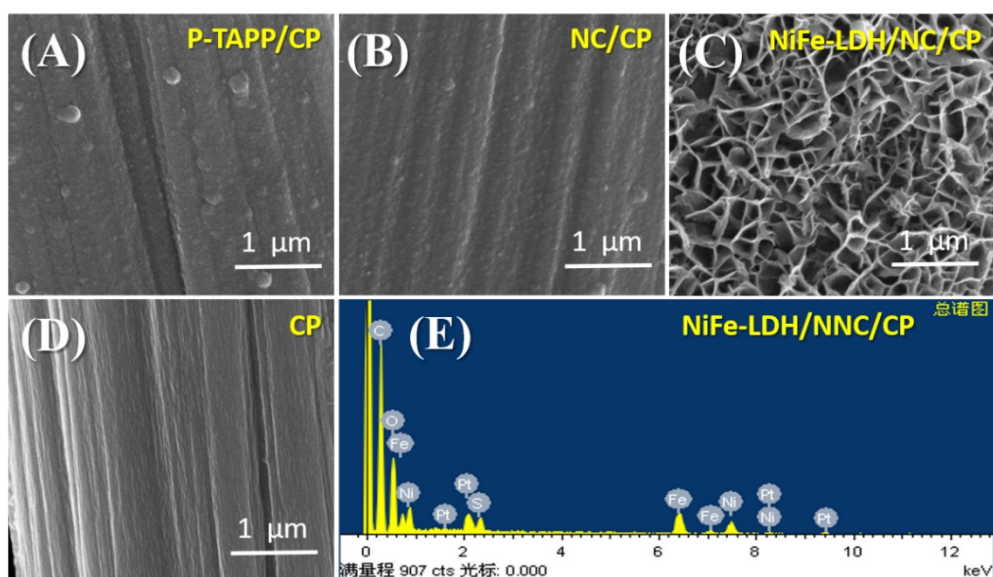**Figure S4.** Optical pictures of as-prepared samples.

Figure S5. A–D) SEM images of the as-prepared P-TAPP/CP, NC/CP, NiFe-LDH/NC/CP, and CP, respectively. E) EDX spectra of the NiFe-LDH/NNC/CP.
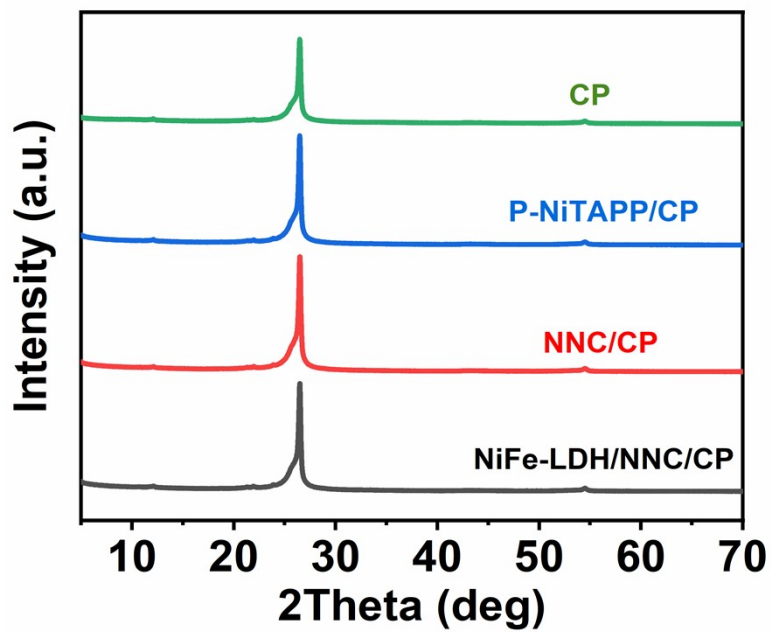
Figure S6. XRD patterns of CP, NiTAPP/CP, NNC/CP, and NiFe-LDH/NNC/CP electrodes.
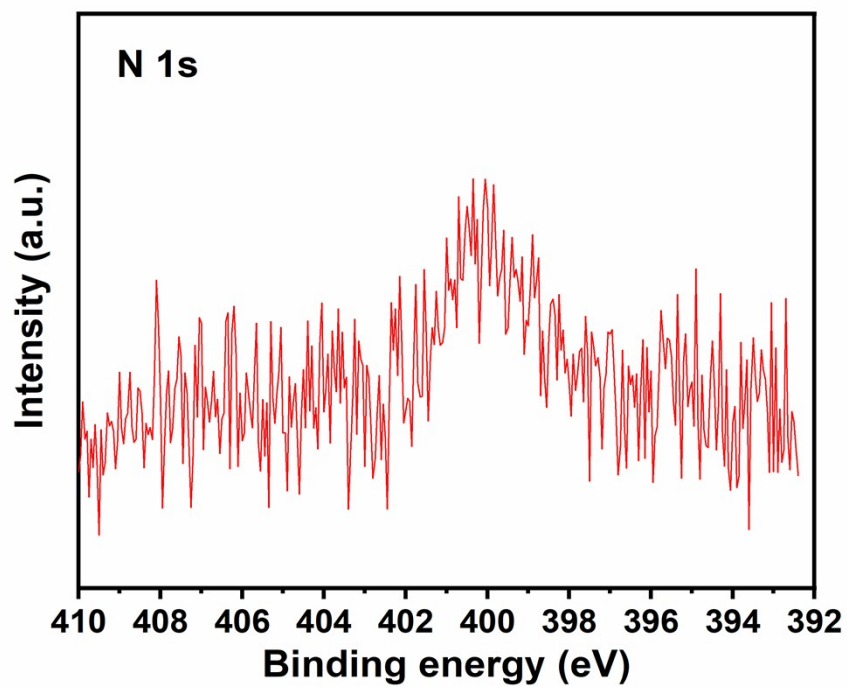

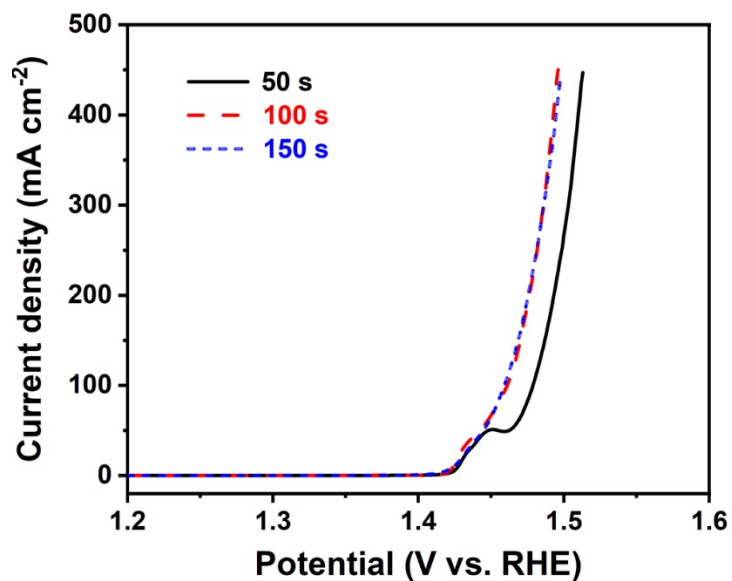**Figure S7.** The XPS spectrum of N 1s for NiFe-LDH/NNC/CP

Figure S8. OER polarization curves of NiFe-LDH/NNC/CP with different electrodeposition time of NiFe-LDH tested in 1 M KOH electrolyte. (Electrode prepared with 100 s is the sample in the manuscript)
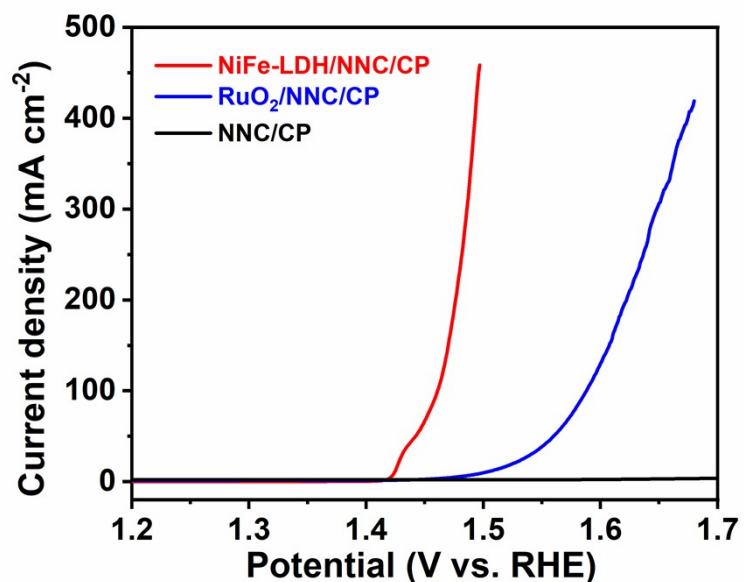

Figure S9. The LSV curves of NiFe-LDH/NNC/CP, RuO$_2$/NNC/CP and NNC/CP. (commercial RuO$_2$ was loaded with 2 mg cm^{-2}, and the RuO$_2$/CP drives a current density of 100 mA cm^{-2} at an overpotential of 358 mV.)
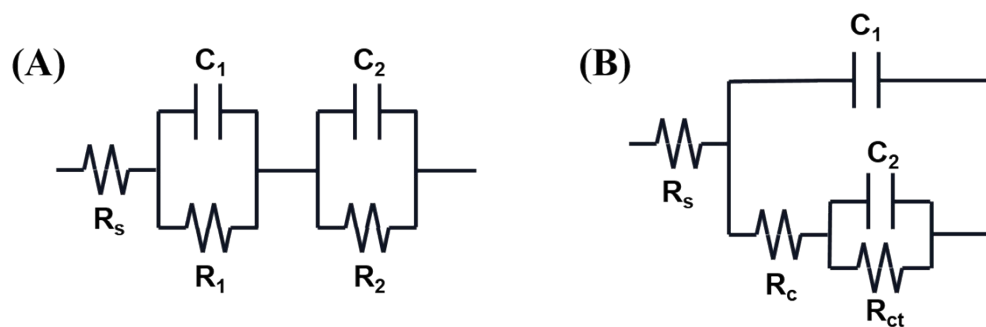
Figure S10. The equivalent circuit diagrams of (A) NiFe-LDH/NNC/CP and NiFe-LDH/NC/CP, (B) NiFe-LDH/CP

Table S2. The fitted value of the resistance in the equivalent circuit.

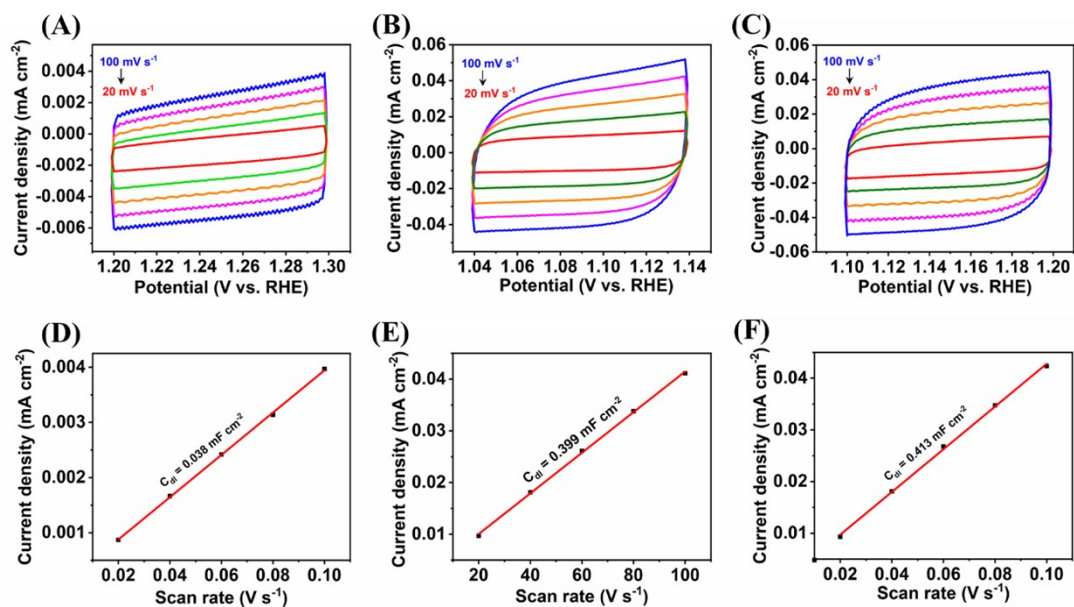|		NiFe-LDH/NNC/CP	NiFe-LDH/NC/CP	NiFe-LDH/CP
R_{ct}	R_1	0.34 Ω	0.54 Ω	20.11 Ω
	R_2	1.08 Ω	1.37 Ω	

Figure S11. Typical cyclic voltammograms at different scan rates of (A) NiFe-LDH/CP, (B) NiFe-LDH/NC/CP, and (C) NiFe-LDH/NNC/CP. Capacitive currents as a function of scan rate for (D) NiFe-LDH/CP, (E) NiFe-LDH/NC/CP, and (F) NiFe-LDH/NNC/CP.
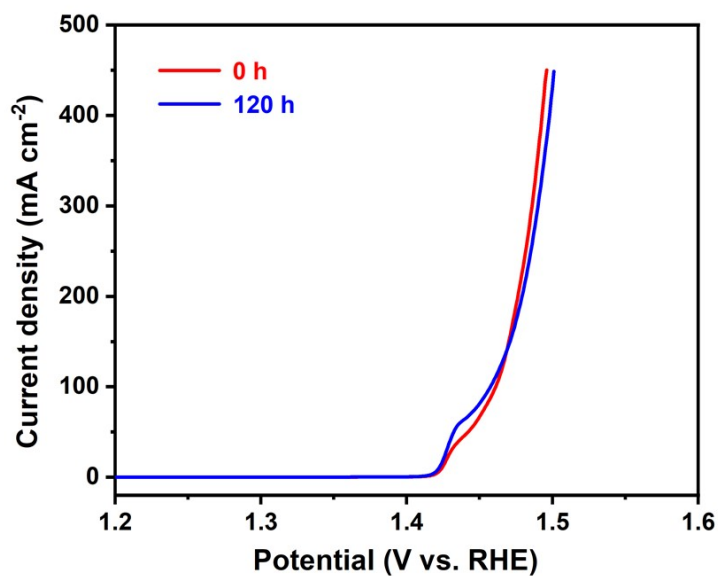

Figure S12. LSV curves of the NiFe-LDH/NNC/CP before and after 120 h of electrolysis with 20 mA cm^{-2}.
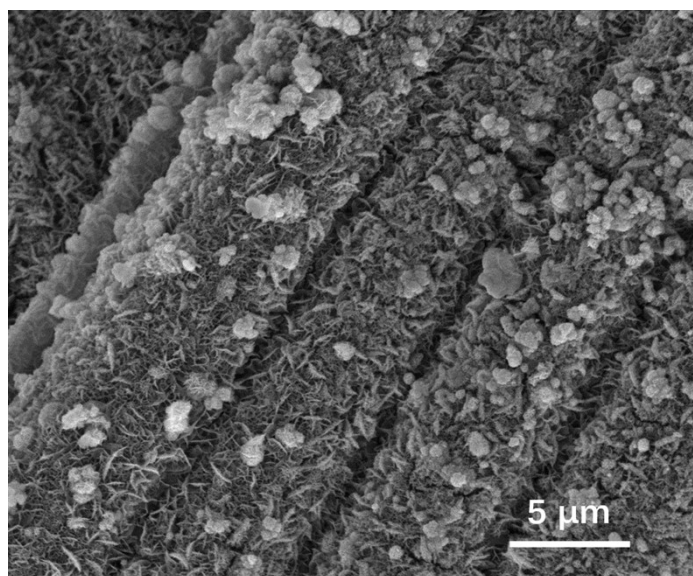
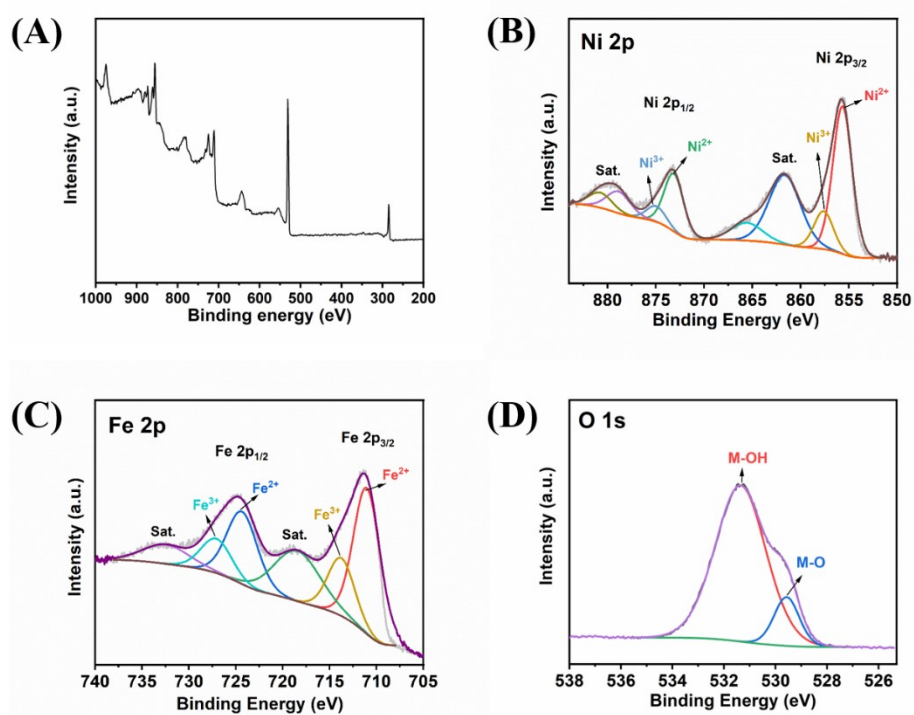**Figure S13.** SEM image of the NiFe-LDH/NNC/CP after electrolysis

Figure S14. (A) Full survey XPS spectra; High-resolution XPS spectra of (B) Ni 2p, (C) Fe 2p and (D) O 1s for NiFe-LDH/NNC/CP after electrolysis

Table S3. Comparison of the OER performance and the methods between the NiFe-LDH/NNC/NF electrode and other recently reported electrodes in 1 M KOH electrolyte.

Catalyst	Overpotential /mV	Tafel slope (mV/dec)	Current collector	Method	Reference
NiFe-LDH/NNC/CP	233	25.8	Carbon paper	Electrodeposition	This work
Cu@NiFe LDH	281	27.8	Cu foam	Electrodeposition	2
NiFeCH(Ce)	252	59	Carbon paper	In situ growth	3
NiCe@NiFe/NF-N	254	59.9	Ni foam	Electrodeposition	4
A-NiFe	251	43	Ni foam	Atmosphere corrosion	5
a-NiFe NS	240	31.8	Ni foam	Liquid corrosion	6
CoS@NiFe LDH/NF	312	49	Ni foam	Electrodeposition	7
Ru/NiFeLDH-F/NF	345	50.2	Ni foam	Hydrothermal/hydrogen reduction	8
NiFe-LDH@CoS$_x$/NF	330	62	Ni foam	Hydrothermal/ Electrodeposition	9
CoNiN@NiFe LDH	290	58.1	Carbon cloth	Dropping	10
NiCo$_{2-x}$Fe$_x$O$_4$	320	42	Ni foam	Electrodeposition	11
CoNiFeO$_x$-NC	286	64.05	carbon paper	Dropping	12
NiFe$_2$O$_{4-x}$/NMO-25	304	42.7	Ni foam	In situ growth	13
CoNi/CoFe$_2$O$_4$/NF	290	45	Ni foam	hydrothermal	14
CoVFeN@NF	264	34.8	Ni foam	In situ growth	15
(Ni$_x$Fe$_{1-x}$)$_2$P	~250	59.3	NiFe foam	Hydrothermal/ phosphating	16
e-ICLDH@GDY/NF	249	43.6	Ni foam	In situ growth	17
S-doped (Ni,Fe)OOH	281	48.9	Ni foam	In situ growth	18
NiMoO$_x$/NiMoS	225	34	Ni foam	In situ growth	19
NiFe LDH@Ni$_3$N/NF	238	61	Ni foam	Electrodeposition	20
Ni@NiFe LDH	269	66.3	Ni foam	Electrodeposition	21
Co$_3$O$_4$@NiFe LDH	269	66	Ni foam	hydrothermal	22
NiFe LDH-NiSe	240	65.6	Ni foam	hydrothermal	23

References

1. E. Tavakoli, A. Kakekhani, S. Kaviani, P. Tan, M. M. Ghaleni, M. A. Zaeem, A. M. Rappe and S. Nejati, *J. Am. Chem. Soc.*, 2019, **141**, 19560-19564.

2. L. Yu, H. Zhou, J. Sun, F. Qin, F. Yu, J. Bao, Y. Yu, S. Chen and Z. Ren, *Energy Environ. Sci.*, 2017, **10**, 1820-1827.

3. J. Cai, J. Huang, S. Xu, L. Yuan, X. Huang, Z. Huang and C. Zhang, *J. Solid State Electrochem.*, 2019, **23**, 3449-3458.

4. G. Liu, M. Wang, Y. Wu, N. Li, F. Zhao, Q. Zhao and J. Li, *Appl. Catal., B*, 2020, **260**, 118199.

5. S. Du, Z. Ren, X. Wang, J. Wu, H. Meng and H. Fu, *ACS Nano*, 2022, **16**, 7794-7803.

6. X. Yang, Q.-Q. Chen, C.-J. Wang, C.-C. Hou and Y. Chen, *J. Energy Chem.*, 2019, **35**, 197-203.

7. Y. J. Lee and S.-K. Park, *Small*, 2022, **18**, 2200586.

8. Y. Wang, P. Zheng, M. Li, Y. Li, X. Zhang, J. Chen, X. Fang, Y. Liu, X. Yuan, X. Dai and H. Wang, *Nanoscale*, 2020, **12**, 9669-9679.

9. Y. Yang, Y. Xie, Z. Yu, S. Guo, M. Yuan, H. Yao, Z. Liang, Y. R. Lu, T.-S. Chan, C. Li, H. Dong and S. Ma, *Chem. Eng. J.*, 2021, **419**, 129512.

10. J. Wang, G. Lv and C. Wang, *Appl. Surf. Sci.*, 2021, **570**, 151182.

11. Y. Huang, S. L. Zhang, X. F. Lu, Z.-P. Wu, D. Luan and X. W. Lou, *Angew. Chem. Int. Ed.*, 2021, **60**, 11841-11846.

12. C. Chen, Y. Tuo, Q. Lu, H. Lu, S. Zhang, Y. Zhou, J. Zhang, Z. Liu, Z. Kang, X. Feng and D. Chen, *Appl. Catal., B*, 2021, **287**, 119953.

13. J. Choi, D. Kim, W. Zheng, B. Yan, Y. Li, L. Y. S. Lee and Y. Piao, *Appl. Catal., B*, 2021, **286**, 119857.

14. S. Li, S. Sirisomboonchai, A. Yoshida, X. An, X. Hao, A. Abudula and G. Guan, *J. Mater. Chem. A*, 2018, **6**, 19221-19230.

15. D. Liu, H. Ai, J. Li, M. Fang, M. Chen, D. Liu, X. Du, P. Zhou, F. Li, K. H. Lo, Y. Tang, S. Chen, L. Wang, G. Xing and H. Pan, *Adv. Energy Mater.*, 2020, **10**, 2002464.

16. S. Sun, X. Zhou, B. Cong, W. Hong and G. Chen, *ACS Catal.*, 2020, **10**, 9086-9097.

17. L. Hui, Y. Xue, B. Huang, H. Yu, C. Zhang, D. Zhang, D. Jia, Y. Zhao, Y. Li, H. Liu and Y. Li, *Nat. Commun.*, 2018, **9**, 5309.

18. L. Yu, L. Wu, B. McElhenny, S. Song, D. Luo, F. Zhang, Y. Yu, S. Chen and Z. Ren, *Energy Environ. Sci.*, 2020, **13**, 3439-3446.

19. P. Zhai, Y. Zhang, Y. Wu, J. Gao, B. Zhang, S. Cao, Y. Zhang, Z. Li, L. Sun and J. Hou, *Nat. Commun.*, 2020, **11**, 5462.

20. B. Wang, S. Jiao, Z. Wang, M. Lu, D. Chen, Y. Kang, G. Pang and S. Feng, *J. Mater. Chem. A*, 2020, **8**, 17202-17211.

21. Z. Cai, X. Bu, P. Wang, W. Su, R. Wei, J. C. Ho, J. Yang and X. Wang, *J. Mater. Chem. A*, 2019, **7**, 21722-21729.

22. S. Wang, J. Wu, J. Yin, Q. Hu, D. Geng and L.-M. Liu, *ChemElectroChem*, 2018, **5**, 1357-1363.

23. S. Dutta, A. Indra, Y. Feng, T. Song and U. Paik, *ACS Appl. Mater. Interfaces*, 2017, **9**, 33766-33774.